A Novel Shadow-Free Feature Extractor for Real-Time Road Detection*

Zhenqiang Ying, Ge Li†, Xianghao Zang, Ronggang Wang, and Wenmin Wang
School of Electronic and Computer Engineering
Shenzhen Graduate School, Peking University, China
zqying@pku.edu.cn,gli@pkusz.edu.cn,zangxh@pku.edu.cn,{rgwang,wangwm}@pkusz.edu.cn

ABSTRACT

Road detection is one of the most important research areas in driver assistance and automated driving field. However, the performance of existing methods is still unsatisfactory, especially in severe shadow conditions. To overcome those difficulties, first we propose a novel shadow-free feature extractor based on the color distribution of road surface pixels. Then we present a road detection framework based on the extractor, whose performance is more accurate and robust than that of existing extractors. Also, the proposed framework has much low-complexity, which is suitable for usage in practical systems.

Keywords

road detection; shadow removal; feature extraction; driver assistance system

1. INTRODUCTION

Road detection constitutes a basis for many intelligent vehicle applications such as lane departure warning and lane keeping assistance. The main task of road detection is to detect the road area from an image captured by a camera mounted behind a car windshield. Although many efforts have been devoted using feature-based methods in this area, most detection methods suffer from the interference of shadow [3]. To overcome those difficulties, some researchers proposed illumination-robust feature extractors [17, 27] while others introduced shadow-free feature extractors [2, 16]. Although the shadow-free feature extractors can help improve the performance of illumination-sensitive road detection, they still cannot perform well in severe shadow conditions. Meanwhile, shadow removal methods, which may perform better, are too time-consuming for the real-time road detection task. In this paper, we propose a low-complexity shadow-free feature extractor with better performance, especially in severe shadow conditions (cf. Fig.1). Besides, we set up a general framework for road detection based on the proposed extractor. Experiments show that road surfaces can be detected accurately and efficiently through our extractor.

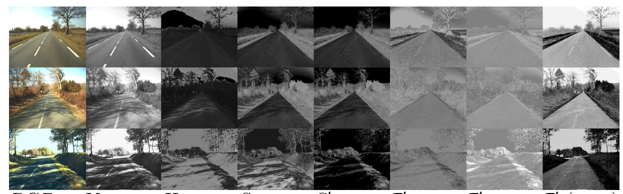

Figure 1: Comparison of various feature extractors. illumination-sensitive: Y. Illumination-robust: H, S and S'. Shadow-free: $\mathcal{I}'_\theta$, $\mathcal{I}'_\alpha$ and $\mathcal{I}'_b(ours)$.

2. RELATED WORK

2.1 Existing Road Detection Methods

Existing road detection techniques can be divided into two broad categories: feature-based [4, 11, 14, 18, 19, 20, 21, 23, 24, 25] and model-based methods [12, 13, 15, 28]. Feature-based methods utilize local visual features of interest, such as gradient, color [11, 18, 20, 22], brightness [21, 24], texture [14], orientation [4] and their combinations [19, 23, 25], which are relatively insensitive to road shapes but are sensitive to illumination effects. Especially, those methods are vulnerable to the interference of severe shadows, which may lead to false alarms in edge detection, texture extraction, color segmentation [3], etc. On the contrary, model-based methods apply global road models to match low-level features, which are more robust against illumination effects but sensitive to road shapes. The reason lies in that the number of predefined models is limited compared to practical scenarios. For example, the geometrical model proposed in [28] contains only thirteen curvatures, which may not match all kinds of road shapes such as *S-curve*. Besides, those methods may totally fail under severe shadow scenarios because of model mismatch. As a conclusion, both existing feature-based and model-based road detection methods suffer from severe shadows, thus a more robust method is critical to real applications.

*This project was supported by Science and Technology Planning Project of Guangdong Province, China (No. 2014B090910001), Shenzhen Peacock Plan (20130408-183003656), China 863 project of 2015AA015905 and Shenzhen Research Project (JCYJ20150331100658943).

†Corresponding author.

MM '16, October 15-19, 2016, Amsterdam, Netherlands
© 2016 ACM. ISBN 978-1-4503-3603-1/16/10…$15.00
DOI: http://dx.doi.org/10.1145/2964284.2967294

2.2 Feature Extractors in Severe Shadow Cases

To fight for the severe shadow interferences, feature extractors are employed in the pre-processing stage to obtain a grayscale feature image, in which illumination effects are reduced. Two kinds of feature extractors are studied: illumination-robust and shadow-free extractors.

Illumination-robust feature extractors. In RGB space, the brightness and color information are mixed together for three components, thus they are vulnerable to the impact of shadow. To solve this problem, color space conversion is often employed [11, 18, 20] to extract the brightness information into a separate component, such as I of HSI, L of Lab and Y of YUV. The remaining two components are suitable for road detection since they only contain color information which is relatively illumination-insensitive. Take HSI as an example, H component can be employed to extract road features [20], and S component is suitable to extract roadside vegetation [26]. However, color components are unstable in severe shadow cases (cf. Fig.1). An illumination-robust feature called *S'* is presented in [27] to accommodate both the severe shadow cases and weak shadow cases.

Shadow-free feature extractors. Since shadows still exist in the extracted component via illumination-robust extractors, the road boundary may not be recovered well in some cases [27]. To completely remove the shadow interferences, some researchers try to find underlying features which are invariant to illumination effects. *Log-chromaticity space (LCS)* [7] is often employed to recover a shadow-free image. Under the condition that an image is captured by a narrow-band camera with approximately *Planckian illumination* and *Lambertian surfaces*, Finlayson *et al.*[7] show that the set of color surfaces of different chromaticities forms parallel straight lines in the LCS. The band-ratio chromaticity is defined as

$$\chi_j = \frac{\rho_q}{\rho_p}, \quad q \epsilon \{1,2,3\}, q \neq p, \quad j = 1,2, \tag{1}$$

where ρ_1, ρ_2 and ρ_3 are matrices respectively representing the red(R), green(G) and blue(B) components of the raw image, p is the index of the normalizing components and index q points to the remaining two components. The shadow-free image $\mathcal{I}$ proposed in [7] is derived from the aforementioned linear relationship as

$$\mathcal{I} = exp(cos\theta \cdot log(\chi_1) + sin\theta \cdot log(\chi_2)), \tag{2}$$

where θ is a camera-dependent parameter.

Álvarez and Ĺopez [2] applied that method to their shadow-free extractor $\mathcal{I}'_\theta$ for road detection. As shown in Eq.3, G is used for normalization ($p = 2; q = 1, 3$) and the outermost exponential operation is removed to improve the speed.

$$\mathcal{I}'_\theta = cos\theta \cdot log(R/G) + sin\theta \cdot log(B/G) \tag{3}$$

Maddern *et al.*[16] proposed another form of illumination invariant imaging and applied it to vision-based localization, mapping and classification for autonomous vehicles. Their extractor $\mathcal{I}'_\alpha$ is defined as

$$\mathcal{I}'_\alpha = (1-\alpha) \cdot log(R) + \alpha \cdot log(B) - log(G) + 0.5, \tag{4}$$

where α is a camera dependent parameter ($\alpha = \frac{sin\theta}{cos\theta + sin\theta}$) and 0.5 is an offset term.

As shown in Fig.1, shadow-free feature extractors perform better than illumination-robust extractors in weak shadow cases since the shadows are completely removed. However, their performance in severe shadow cases still needs to be improved. To find why existing shadow-free extractors [2, 16] fail in severe shadow cases, we choose a shadowy road image from ROMA dataset [21] and then map pixels of road and vegetation regions into LCS. According to their basic assumption, the set of color surfaces of different chromaticities will form parallel straight lines in LCS. However, the distribution is more like a quadratic function in severe shadow conditions, and the two classes are mixed together indistinguishably (cf. Fig.2 (left)).

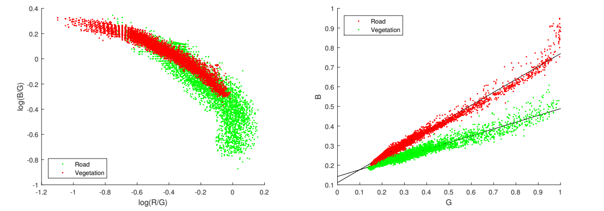

Figure 2: Road and vegetation pixels on $log\frac{R}{G}$-$log\frac{B}{G}$ (left) and G-B (right) plane.

3. OUR APPROACH

To obtain a new shadow-free feature extractor which is robust against severe shadows, a more proper relationship is required. Healey *et al.*[10] proved that the measured colors of homogeneous dielectric surfaces lie on a line passing through the origin of RGB space. To verify that, we map the road and vegetation pixels from aforementioned shadowy road image into RGB space. Since road and vegetation can be treated as homogeneous dielectric surfaces, their corresponding pixels should be arranged in line shapes. Our experimental results are in agreement with [10] except for an offset between the intersection and origin (cf. Fig.3).

To see the offset more clearly, we project the pixels onto the GB plane (cf. Fig.2 (right)), where the G and B components of the same material are distributed along a straight line with an offset shown as the intercept of B axis. That offset is ignored in [10]. We can use a linear function to accurately describe the relationships among road surface pixels as

$$G_{r,c} \approx k * B_{r,c} + b, \quad (r,c) \in road, \tag{5}$$

where r and c are the indexes of row and column indicating the location of a road pixel, k is the slope of the straight line and b is the intercept.

Define a matrix K as

$$K \triangleq \frac{G-b}{B}, \tag{6}$$

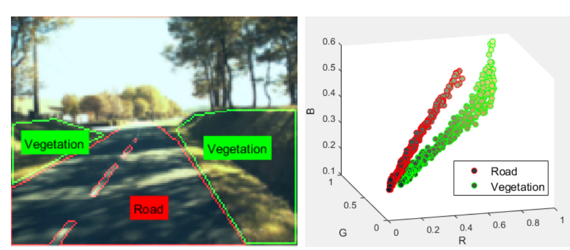

Figure 3: Road and vegetation pixels in RGB space.

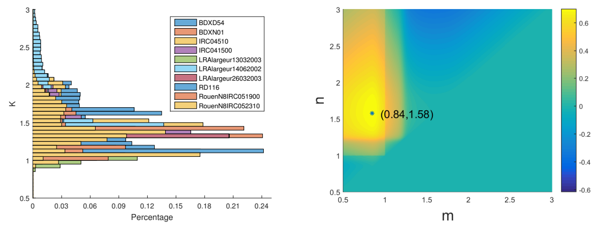

Figure 4: Histogram of K (left) and the optimal range (m^*, n^*) for ROMA dataset (right).

whose elements in the road area are approximately a constant (cf. Eq.7). The intercept b can be obtained by polynomial fitting among the road pixels on *GB* plane. Besides, experiments show that all images captured by the same camera can share one b, so b can be explained as an intrinsic parameter of each color camera like θ of $\mathcal{I}'_\theta$ (Eq.3) and α of $\mathcal{I}'_\alpha$ (Eq.4). Therefore, we only need to do an off-line calibration once for one camera.

$$\forall (r,c) \in road \rightarrow K_{r,c} = \frac{G_{r,c} - b}{B_{r,c}} \approx k \tag{7}$$

To design an efficient extractor, we need to analyze the distribution of K. For each sub-dataset of ROMA, we plot the histogram of K to each pixel in all images as shown in Fig.4 (left). Let K_{min} and K_{max} be the minimum and maximum of K. Unevenly distributed of K makes it inefficient to use the whole range $[K_{min}, K_{max}]$ to form the shadow-free component. Thus, we need to choose a dominant subrange (m, n) to make it more compact.

Let $\mathcal{H}$ be the overall histogram of ROMA dataset. We compute the optimal range $[m^*, n^*] \subset [K_{min}, K_{max}]$ for ROMA dataset via

$$(m^*, n^*) = \underset{(m,n)}{\operatorname{argmax}}\{g(m,n) - c(m,n)\}, \tag{8}$$

where $g(m,n)$ is defined as

$$g(m,n) \triangleq \sum_{i=m}^{n} \mathcal{H}(i) / \sum_{i=K_{min}}^{K_{max}} \mathcal{H}(i), \tag{9}$$

and $c(m,n)$ is defined as

$$c(m,n) \triangleq (m-n)/(K_{max} - K_{min}). \tag{10}$$

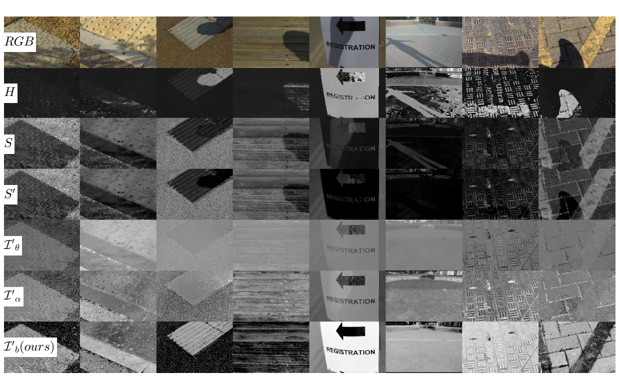

Figure 5: Shadowy images and the results of extractors. Complete results can be found on our website.

We find that the optimal range for ROMA dataset is $[m^*, n^*] = [0.84, 1.58]$, as shown in Fig.4 (right). To facilitate normalization (cf. Eq.11) and make our extractor more concise, $[m, n] = [1, 2]$ are used to approximate the $[m^*, n^*]$ and our extractor $\mathcal{I}'_b$ is derived (cf. Eq.12).

$$1 \leqslant K \leqslant 2 \Rightarrow 0 \leqslant 2 - K \leqslant 1 \tag{11}$$

$$\mathcal{I}'_b \triangleq 2 - K \tag{12}$$

To apply our extractor to road detection task, we present a general road detection framework based on feature extractors. The framework takes an *RGB* image as input and outputs a binary image where 1 denotes road pixel and 0 denotes non-road pixel. Our road detection framework is summarized as follows:

1. Region of interest (ROI) determination. Limit the following processing in ROI to avoid meaningless opera tions on irrelevant regions.
2. Feature Extraction. Apply an extractor to the image in ROI and output a grayscale image.
3. Filtering. Remove the noise introduced when performing feature extraction.
4. Segmentation. Segment the grayscale image into several regions (set of pixels) and output a labeled image.
5. Connected Component Analysis. Find the region with the largest area (cardinality of set) and output a binary image indicating that region.
6. Morphological Filtering. Applying morphology image operation using a structuring element to separate the road from other areas.
7. Holes filling. Road markings will produce holes in the obtained area. Filling the holes to obtain a complete road area.

4. EXPERIMENTAL RESULTS

4.1 Shadow-Free Extractor

Effectiveness. We test our extractor on a public dataset [9]. Different from all other extractors, our results look like a natural image except that the shadows are disappeared. As sample images shown in Fig. 6, our extractor is robust against images of a wide range of materials and surface textures. It also retains the texture (e.g. road, brick and wood) and details (e.g. handwriting) well compared to other extractors, as shown in Fig.5.

Time Efficiency. We measure the average time and variance ($\mu \pm \sigma$) for extractors implemented with MATLAB to process an image having 1280×1024 dots with a PC equipped with an i7-3770 3.40 GHz CPU and 16GB RAM (GPU acceleration is not used). Due to the low-complexity of our extractor, it achieves the fastest speed compared with others (cf. Table 1).

Table 1: Processing speed of feature extractors.

Extractors	S' [27]	$\mathcal{I}'_\theta$ [2]	$\mathcal{I}'_\alpha$ [16]	$\mathcal{I}'_b$ (Ours)
Time/ms	21.3±0.2	52.2±0.4	54.9±3.6	**12.9±0.1**

Table 2: Pixel-wise measures (right) defined using entries of a contingency table (left).

		Ground-truth: Others	Ground-truth: Road
Result	Others	TN	FN
	Road	FP	TP

Measure	Definition
Quality	$\hat{g} = \frac{TP}{TP+FP+FN}$
Precision	$DR = \frac{TP}{TP+FP}$
Recall	$DA = \frac{TP}{TP+FN}$
Effectiveness	$F = \frac{2DR \times DA}{DR+DA}$
Valid	$VRI = \frac{TP+TN}{TP+TN+FP+FN} \geq 0.8$

4.2 Road Detection

To evaluate the performance of road detection, we adopt pixel-wise measurements shown in Table 2. Quantitative evaluations are provided using four error measurements: quality $\hat{g}$, precision DR (also known as detection rate), recall DA (also known as detection accuracy) and effectiveness F. We also use a qualitative measurement called valid road result index VRI [1]: a detection result is valid ($VRI = 1$) if and only if at least 80% of pixels are correctly classified. As [1] suggested, road boundary pixels should be discarded when computing those measurements to reduce the inherent error of manual segmentation.

ROMA dataset. There are 10 sub-datasets of various scenes, road types and illumination conditions in ROMA.We manually labeled road area ground truth of all sub-datasets. To make a fair comparison, different extractors are employed in the same road detection framework under the same parameter settings. In our implementation, the lower half of image is selected as ROI in step 1. A graph-based image segmentation algorithm introduced in [6] with the parameters $\sigma = 1.2$, $k = 300$ and $min = 1000$ is employed in step 4. Since the algorithm already has a parameter σ to smooth the image, a 5×5 median filter is employed in step 3 to filter the extracted feature image. Finally, morphology opening using a structuring element of 8×8 disk is applied in step 6 to separate the road from other areas. As shown in Table 3, detection results based on the proposed extractor outperform the others in both quantitative and qualitative measurements, especially in adverse lighting conditions.

KITTI-ROAD dataset [8]. To test the performance on challenging KITTI-ROAD dataset, we compare our result with that of the state-of-art top 3 methods accessible on the KITTI benchmark website[1]. As shown in Fig.6, our detection result shows more accuracy than that of the state-of-art methods. Besides, we test three edge detectors (Sobel, Canny and Structured Edge [5]) in severe shadow cases. As shown in Fig.7, using the shadow-free image obtained by our extractor can achieve a better result. Also, the false color segmentation caused by severe shadow can be avoided by employing our extractor as a preprocessing step, as shown in Fig.8.

To encourage future works, we make the source code open, as well as our labeled ground-truth for ROMA. More testing results can be found on our project website[2].

Table 3: Performance on ROMA Dataset.

	$\hat{g}$	DR	DA	F	VRI
	Complete dataset				
Y	.79 ± .17	.91 ± .12	.86 ± .17	.87 ± .12	63%
S' [26]	.85 ± .18	.94 ± .11	.90 ± .17	.91 ± .12	75%
$\mathcal{I}'_\theta$ [2]	.82 ± .23	.94 ± .12	.87 ± .23	.88 ± .18	72%
$\mathcal{I}'_\alpha$ [16]	.79 ± .14	.83 ± .13	.95 ± .11	.87 ± .09	59%
$\mathcal{I}'_b$ (Ours)	**.92±.11**	**.96±.07**	**.96±.09**	**.96±.07**	**93%**
	Adverse lighting conditions				
Y	.76 ± .16	.88 ± .14	.85 ± .18	.85 ± .12	48%
S' [26]	.81 ± .20	.91 ± .14	.88 ± .19	.88 ± .14	67%
$\mathcal{I}'_\theta$ [2]	.81 ± .20	.93 ± .11	.87 ± .21	.88 ± .14	65%
$\mathcal{I}'_\alpha$ [16]	.77 ± .14	.81 ± .14	.95 ± .10	.86 ± .09	48%
$\mathcal{I}'_b$ (Ours)	**.92±.09**	**.96± .07**	**.96±.07**	**.96±.05**	**96%**

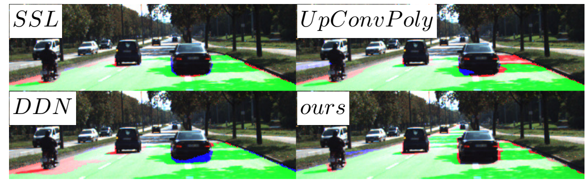

Figure 6: Comparison with state-of-art methods. Red areas denote false negatives, blue areas correspond to false positives and green areas represent true positives.

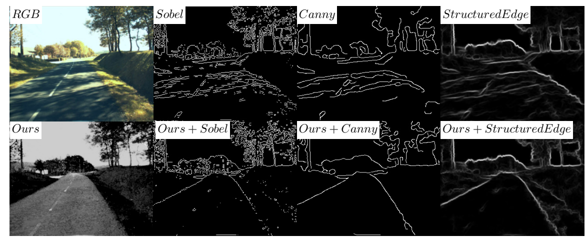

Figure 7: Improve edge detection via our extractor.

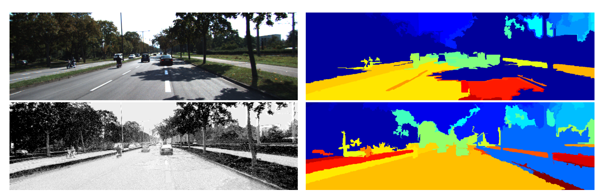

Figure 8: Improve segmentation via our extractor.

5. CONCLUSIONS

In this paper, we propose a novel shadow-free feature extractor to improve the performance of road detection under severe shadow conditions. The proposed extractor shows robustness against different materials and illumination conditions. A road detection framework based on the proposed extractor is built. Experimental results on public datasets demonstrate the superior performance compared to other existing extractors. As a result, the novel extractor is well suitable to other computer vision tasks as well as autonomous driving applications by its good performance and computational efficiency.

[1] http://www.cvlibs.net/datasets/kitti/eval_road.php
[2] https://github.com/baidut/OpenVehicleVision/

6. REFERENCES

[1] J. M. Álvarez, T. Gevers, and A. M. Lopez. 3d scene priors for road detection. In *Computer Vision and Pattern Recognition (CVPR), 2010 IEEE Conference on*, pages 57–64. IEEE, 2010.

[2] J. M. Álvarez and A. M. Ĺopez. Road detection based on illuminant invariance. *Intelligent Transportation Systems, IEEE Transactions on*, 12(1):184–193, 2011.

[3] A. Bar Hillel, R. Lerner, D. Levi, and G. Raz. Recent progress in road and lane detection: a survey. *Machine Vision and Applications*, 25(3):727–745, 2014.

[4] B. Benligiray, C. Topal, and C. Akinlar. Video-based lane detection using a fast vanishing point estimation method. In *Multimedia (ISM), 2012 IEEE International Symposium on*, pages 348–351, Dec 2012.

[5] P. Dollár and C. Zitnick. Structured forests for fast edge detection. In *Proceedings of the IEEE International Conference on Computer Vision*, pages 1841–1848, 2013.

[6] P. F. Felzenszwalb and D. P. Huttenlocher. Efficient graph-based image segmentation. *International Journal of Computer Vision*, 59(2):167–181, 2004.

[7] G. D. Finlayson, S. D. Hordley, C. Lu, and M. S. Drew. On the removal of shadows from images. *Pattern Analysis and Machine Intelligence, IEEE Transactions on*, 28(1):59–68, 2006.

[8] J. Fritsch, T. Kuhnl, and A. Geiger. A new performance measure and evaluation benchmark for road detection algorithms. In *Intelligent Transportation Systems-(ITSC), 2013 16th International IEEE Conference on*, pages 1693–1700. IEEE, 2013.

[9] H. Gong and D. Cosker. Interactive shadow removal and ground truth for variable scene categories. In *BMVC 2014-Proceedings of the British Machine Vision Conference 2014*. University of Bath, 2014.

[10] G. Healey. Segmenting images using normalized color. *Systems, Man and Cybernetics, IEEE Transactions on*, 22(1):64–73, 1992.

[11] J. Huang, B. Kong, B. Li, and F. Zheng. A new method of unstructured road detection based on hsv color space and road features. In *Information Acquisition, 2007. ICIA '07. International Conference on*, pages 596–601, July 2007.

[12] S.-N. Kang, S. Lee, J. Hur, and S.-W. Seo. Multi-lane detection based on accurate geometric lane estimation in highway scenarios. In *Intelligent Vehicles Symposium Proceedings, 2014 IEEE*, pages 221–226, June 2014.

[13] Z. Kim. Robust lane detection and tracking in challenging scenarios. *Intelligent Transportation Systems, IEEE Transactions on*, 9(1):16–26, March 2008.

[14] H. Kong, J.-Y. Audibert, and J. Ponce. General road detection from a single image. *Image Processing, IEEE Transactions on*, 19(8):2211–2220, 2010.

[15] Z. Li, Z. xing Cai, J. Xie, and X. ping Ren. Road markings extraction based on threshold segmentation. In *Fuzzy Systems and Knowledge Discovery (FSKD), 2012 9th International Conference on*, pages 1924–1928, May 2012.

[16] W. Maddern, A. Stewart, C. McManus, B. Upcroft, W. Churchill, and P. Newman. Illumination invariant imaging: Applications in robust vision-based localisation, mapping and classification for autonomous vehicles. In *Proceedings of the Visual Place Recognition in Changing Environments Workshop, IEEE International Conference on Robotics and Automation (ICRA), Hong Kong, China*, 2014.

[17] C. Oh, J. Son, and K. Sohn. Illumination robust road detection using geometric information. In *Intelligent Transportation Systems (ITSC), 2012 15th International IEEE Conference on*, pages 1566–1571. IEEE, 2012.

[18] C. Rotaru, T. Graf, and J. Zhang. Color image segmentation in hsi space for automotive applications. *Journal of Real-Time Image Processing*, 3(4):311–322, 2008.

[19] T. Scharwachter and U. Franke. Low-level fusion of color, texture and depth for robust road scene understanding. In *Intelligent Vehicles Symposium (IV), 2015 IEEE*, pages 599–604. IEEE, 2015.

[20] T.-Y. Sun, S.-J. Tsai, and V. Chan. Hsi color model based lane-marking detection. In *Intelligent Transportation Systems Conference, 2006. ITSC '06. IEEE*, pages 1168–1172, Sept 2006.

[21] T. Veit, J.-P. Tarel, P. Nicolle, and P. Charbonnier. Evaluation of road marking feature extraction. In *Intelligent Transportation Systems, 2008. ITSC 2008. 11th International IEEE Conference on*, pages 174–181, Oct 2008.

[22] B. Wang, V. Frémont, and S. A. Rodríguez. Color-based road detection and its evaluation on the kitti road benchmark. In *Intelligent Vehicles Symposium Proceedings, 2014 IEEE*, pages 31–36. IEEE, 2014.

[23] J. Wang, Z. Ji, and Y.-T. Su. Unstructured road detection using hybrid features. In *Machine Learning and Cybernetics, 2009 International Conference on*, volume 1, pages 482–486. IEEE, 2009.

[24] J. Wang, T. Mei, B. Kong, and H. Wei. An approach of lane detection based on inverse perspective mapping. In *Intelligent Transportation Systems (ITSC), 2014 IEEE 17th International Conference on*, pages 35–38, Oct 2014.

[25] Y. U. Yim and S. young Oh. Three-feature based automatic lane detection algorithm (tfalda) for autonomous driving. *Intelligent Transportation Systems, IEEE Transactions on*, 4(4):219–225, Dec 2003.

[26] Z. Ying and G. Li. Robust lane marking detection using boundary-based inverse perspective mapping. In *2016 IEEE International Conference on Acoustics, Speech and Signal Processing (ICASSP)*, pages 1921–1925, March 2016.

[27] Z. Ying, G. Li, and G. Tan. An illumination-robust approach for feature-based road detection. In *2015 IEEE International Symposium on Multimedia (ISM)*, pages 278–281, Dec 2015.

[28] S. Zhou, Y. Jiang, J. Xi, J. Gong, G. Xiong, and H. Chen. A novel lane detection based on geometrical model and gabor filter. In *Intelligent Vehicles Symposium (IV), 2010 IEEE*, pages 59–64, June 2010.